doi:10.2533/chimia.2024.326 Chimia 78 (2024) 326–332

Current Developments in *Operando* Electron Paramagnetic Resonance Spectroscopy

Jörg Fischer, Mikhail Agrachev, Jörg Forrer, Rene Tschaggelar, Oliver Oberhänsli, and Gunnar Jeschke*

Abstract: Electron paramagnetic resonance (EPR) spectroscopy is a powerful tool for *in situ*/*operando* tracking of catalytic reactions that involve paramagnetic species either as a catalyst (*e.g.* transition metal ions or defects), reaction intermediates (radicals) or poisoning agents such as coke. This article provides a summary of recent experimental examples and developments in resonator design as well as detection schemes that were carried out in our group. Opportunities for applying this technique are illustrated by examples, including studies of transition metal exchanged zeolites and metal-free zeolites as well as metal oxide catalysts. The inherent limitations of EPR applied at high temperatures are discussed, as well as strategies in reducing or lifting these restrictions are evaluated and ideas for future improvements and methodologies are discussed.

Keywords: Defect sites · EPR instrumentation · *Operando* spectroscopy · Transition metal ions

Jörg Fischer was born in Darmstadt (Germany) in 1994 and studied chemistry in Konstanz. Research stays during his master's program included a project in Seattle in the group of Prof. Stoll working on pulsed EPR spectroscopy and in Tübingen in the group of Dr. Berthold focusing on ceramic pigments from the chalcolithic age. After completing his master's studies in 2020 he moved to ETH Zurich where he is currently a PhD student in the Jeschke lab working on methodology development for *operando* EPR spectroscopy.

Mikhail Agrachev was born in Moscow (Russia) in 1988. He received his master's degree in Chemistry at the University of Padova (Italy) and his PhD in Molecular Sciences in 2018, at the same University, with a thesis on the fundamental properties of molecular gold nanoclusters, mainly investigated by EPR. From 2020 he has been working as a post-doc at ETH Zurich in the Jeschke lab. His work is focused on CW and pulsed EPR methods applied to catalysis, material science and magnetism.

Rene Tschaggelar was born in Zurich (Switzerland), finished his degree in electronics in 1982, and later continued to study at ETH Zurich, where he obtained a degree in physics in 1996. After working on industrial projects for 11 years, he took the responsibility for the hardware in the Jeschke lab, where he focuses on resonator design and spectrometer development.

*Correspondence: Prof. Dr. G. Jeschke, E-mail: gjeschke@ethz.ch, Department of Chemistry and Applied Biosciences, ETH Zurich, Zurich, CH-8093 Zurich

Jörg Forrer is a senior electronic engineer with live long experience in the field of high frequency technology. He is an expert in the field of ESR instrumentation. He is a life senior member of the IEEE and was co-founder of the IEEE Swiss microwave chapter MTT-S.

Oliver Oberhänsli was born in Zurich (Switzerland) in 1977. He finished his apprenticeship as a machine mechanic in 1998. In 2014 he obtained his bachelor's degree as a mechanical engineer at Juventus Schulen Zurich. Since 2010, he has worked as a mechanical engineer in the Jeschke lab at ETH Zurich. He is mainly involved in designing and manufacturing new EPR resonators or developing them further.

Gunnar Jeschke was born in Cottbus (Germany) in 1966. He studied chemistry at TU Dresden and holds a doctoral degree from ETH Zurich. He worked on photochemistry at RIKEN (Wako-shi, Japan), solid-state NMR of inorganic materials at University of Bonn (Germany), EPR methods in polymer science and structural biology at MPI for Polymer Research Mainz (Germany) and on theory, instrumentation, and method development in EPR at University of Konstanz (Germany) and ETH Zurich (since 2008). Further interests include ensemble modelling of partially disordered proteins by integrating experimental constraints obtained with different techniques.

1. Introduction

Electron paramagnetic resonance spectroscopy (EPR) is a powerful tool for tracing the oxidation state of metal centers, the formation of organic radicals (*e.g.* coke), and the fate of vacancies

under realistic reaction conditions.[1-4] However, EPR has a seemingly large limitation, namely that only species that carry unpaired electron(s) are detectable.

In the simplest case, the degenerate m_s levels of an $S = 1/2$ system ($m_s = -1/2$ and $m_s = +1/2$) (*e.g.* Cu^{2+}) are split by the Zeeman interaction in the presence of an external magnetic field.

The spectral position and shape of the resulting spectrum is influenced by (1) the surrounding nuclei, (2) the energy of the single-occupied molecular orbital (SOMO) relative to other orbitals, (3) the wavefunction of the SOMO. In systems with more than one unpaired electron (*e.g.* Fe^{3+}) the energy levels are further influenced by the interaction between the electrons, leading to at least partial lifting of the energy degeneracy in the absence of an external magnetic field. This zero-field splitting makes EPR sensitive to the number of unpaired electrons allowing it to detect the difference between low- and high-spin states of the same element. For integer spin systems in the absence of axial symmetry, the zero-field splitting completely lifts level degeneracy, which in combination with the typically fast relaxation means that these ions cannot be measured under standard conditions.[5,6] Therefore, only Kramers ions with half-integer value of the spin quantum number can usually be measured with standard spectrometers.

A summary of detectable ions can be found in Table 1.[4] Many of these paramagnetic species are commonly present in heterogeneous catalysts, and monitoring their structural modifications and redox dynamics during the reaction with *operando* EPR is extremely important for the mechanistic understanding of the catalytic process. EPR can therefore provide detailed insights into the nature of active sites and transient intermediates, and thereby enhance our understanding of catalytic mechanisms. Because some catalytically active species are EPR silent, the technique is often applied in conjunction with other techniques.

The EPR spectrum is traditionally recorded at a fixed microwave frequency while sweeping the external magnetic field through the transition. Thus, one can employ resonant cavities for enhancing the signal. Historically, the frequency bands are labeled with letters that come from radar technology. Frequencies around 9-10 GHz are labeled as X-band and around 32-34 GHz as Q-band.

The limitation of EPR to certain oxidation states can be turned into an advantage in terms of selectivity, leading to unambiguous confirmation of the presence of certain oxidation states and of radical species. Due to this unique sensitivity EPR can be applied to various media and composition feeds since non-paramagnetic species and short-lived intermediates do not contribute to the overall signal. This simplifies the spectra and allows the detection of a small fraction of paramagnetic species, which may happen to be the active sites.

2. *Operando* EPR at ETH Zurich

The idea that time-resolved EPR measurements should be performed under catalytically relevant conditions was already present in the early 70's. In many cases, product detection was omitted, so that these studies would now be called '*in situ*' rather than '*operando'*. Most of the early examples focused on *in situ* formation of organic, mainly aromatic and polyaromatic radicals in zeolites and other catalytic materials.[7-11]

The modern *operando* EPR spectroscopy methodology is largely based on the pioneering work by the Brückner lab, which included the development of several powerful multi-technique setups, combining EPR with electrochemistry, XAS, UV-vis and Raman spectroscopies and applying them to several reactions in heterogeneous, homogeneous, photo- and electrocatalysis.[4,12-14] Seminal contributions to the field of *operando* EPR also include the work of the Mossin lab[15,16] in heterogeneous catalysis at the solid-gas interface as well as work from the Roessler lab and the Schnegg lab in electrochemistry.[17,18]

Table 1. Relevant transition metal ions for *in situ/operando* EPR in their high-spin configuration

d^1 (S = 1/2)	d^3 (S = 3/2)	d^5 (S = 5/2)	d^7 (S = 3/2)	d^9 (S = 1/2)
V^{4+}	Mn^{4+}	Mn^{2+}	Ni^{3+}	Ni^{1+}
Mo^{5+}	Mo^{3+}	Fe^{3+}	Rh^{2+}	Rh^{0}
Cr^{5+}	Cr^{3+}	Cr^{+}	Pd^{3+}	Pt^{+}
Ti^{3+}	Ru^{+}	Ru^{3+}	Co^{2+}	Pd^{+}
$Zr3^{+}$	Ir^{2+}	Ir^{4+}	-	Ag^{2+}
Ce^{3+}	-	-	-	Au^{2+}
-	-	-	-	Cu^{2+}

2.1 *Early Operando EPR at ETH*

The first high-temperature EPR measurements on catalytically-relevant samples were performed in our group in the context of an investigation of lignin pyrolysis.[19,20] Different catalysts were explored, namely nonporous silica and zeolite catalysts (silicalite, HZSM5 and HUSY), in order to unravel the effect of specific surface area, as well as concentration and type of acid sites on stabilizing the aromatic radicals. The evolution of the EPR signal due to aromatic radicals formed from lignin decomposition has been monitored *in situ* at different temperatures (623 K – 823 K). The main result was that the concentration of radicals is significantly higher in the presence of zeolites, compared to pure lignin, clearly showing the role of the inorganic surface in stabilizing the radical species. For these experiments, a home-built, water-cooled resonator was used for the first time, described in detail in section 3.2.

The first *operando* EPR study concerned the propane oxychlorination reaction, where $CrPO_4$ and EuOCl were used as catalysts.[21] In the starting material, Cr and Eu are both prevalently present in the M^{+3} oxidation state, which corresponds to an EPR active S=3/2 state for Cr^{3+} and an EPR-silent non-Kramers S=3 configuration for Eu^{3+}. Partial reduction of the transition metal centers is expected during the reaction, leading to EPR-silent Cr^{2+} defects (S=2) and EPR-active Eu^{2+} defects (S=7/2), respectively. We were able to detect this process with EPR, by monitoring the decrease of Cr^{3+} and the increase of Eu^{2+} signals (Fig. 1a-c). During the continuous acquisition of EPR spectra, the reaction products were detected with a mass spectrometer. Analysis of the combined EPR and MS data showed that the space-time yield (STY) of the reaction strongly correlates with the amount of Cr^{2+} and Eu^{2+} formed. This study paved the way for the investigation of a large number of different reactions. Most of the subsequent studies focused on transition metals and on the monitoring and quantification of their oxidation states.

In parallel, the methodology was refined, and new approaches were developed in order to get more detailed structural and mechanistic information. Also, new features were recently implemented in the experimental setup:

- The possibility to apply high pressures (up to 10 bar) was added. This is achieved by regulating the reaction gas flow with mass flow controllers and adjusting the pressure inside the resonator with a back-pressure regulator at the output of the reactor.

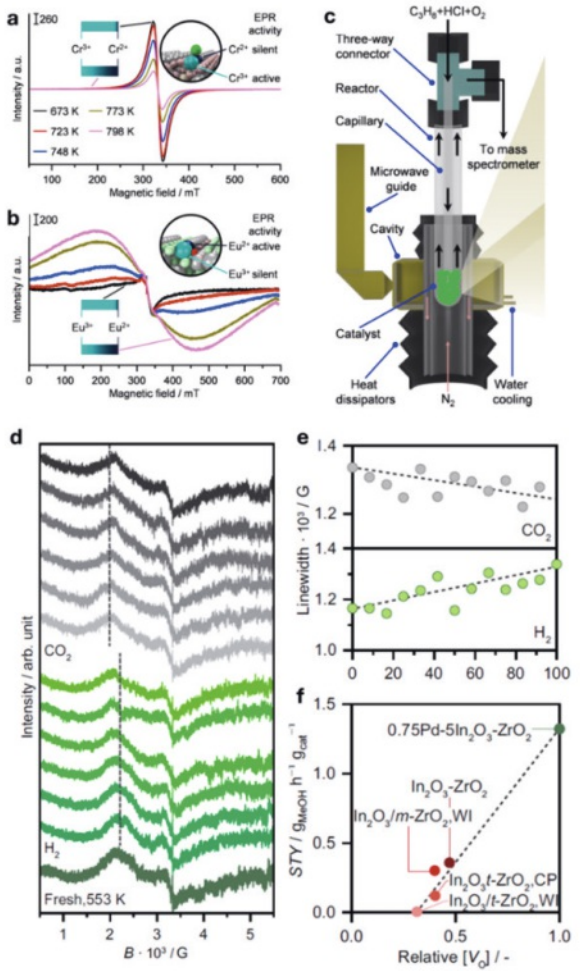

Fig. 1. *Operando* EPR for correlating paramagnetic sites with space-time-yield (STY). Panels a-c refer to propane oxychlorination and panels d-f to methanol formation by CO_2 hydrogenation. a) Variable-temperature *operando* EPR spectra of a $CrPO_4$ catalyst; b) Variable-temperature *operando* EPR spectra of an EuOCl catalyst. c) Single-cavity resonator and reactor configuration. (adapted with permission from [21]). d) *in situ* EPR spectra of a 0.75Pd-5In_2O_3-ZrO_2 catalyst prepared by flame-spray pyrolysis measured first under flowing H_2 (100 min) and then CO_2 (100 min). e) Peak-to-peak linewidth values over time derived from EPR spectra shown in d. f) Methanol STY over the 0.75Pd-5In_2O_3-ZrO_2 catalyst and reference materials as a function of the relative concentration of oxygen vacancies ([VO]), which was derived from the peak-to-peak linewidth of the newly formed signal (adapted from [22]).

- The possibility to perform batch reactions under low-pressure conditions was achieved, by connecting the sample cell to a vacuum line.
- Fast switching between different gases was made possible by digitally-controlled mass flow controllers, allowing modulated excitation *operando* experiments.

2.2 *Zeolite Catalysts*

Several *operando* EPR projects in our group deal with metal-exchanged and undoped zeolite catalysts. A study on methane oxidation by Cu-exchanged mordenite highlights the unique ability of EPR to distinguish structurally different metal sites and thus, in an *operando* context, differentiate their reactivity and eventually identify the active sites.[23] Specifically, different bare Cu^{2+} and $[CuOH]^+$ ions coordinated inside the zeolite channels were identified with EPR. Cu^{2+} is EPR active (d^9, S=1/2) and can be easily assigned because of the hyperfine splitting due to the interaction with the Cu nuclei (I=3/2). The reduced Cu^+ is instead strictly EPR-silent (d^{10}, S=0), which allows to monitor Cu^{2+} reduction *in situ*. Although the bare Cu^{2+} sites were previously assumed to be redox-inert and thus inactive, our *operando* EPR measurements (Fig. 2a-b) clearly demonstrated that they undergo significant reduction during the reaction. Furthermore, it has been shown that, together with the dimeric $[Cu_2O]^{2+}$ species (which are EPR-silent and were monitored by *operando* UV-vis spectroscopy) these sites explain the decay of methane pressure due to two different first-order reactions.

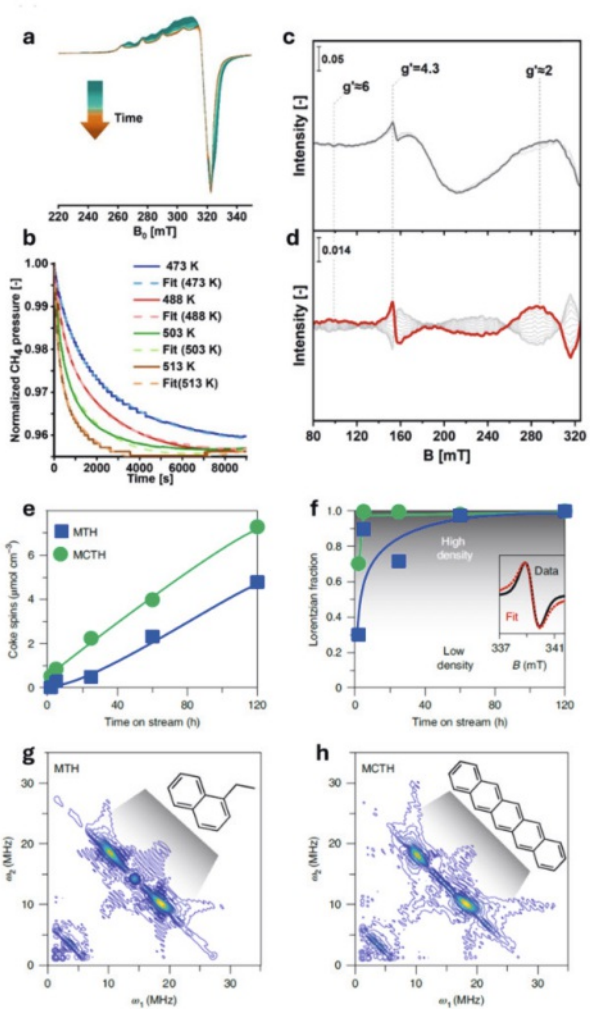

Fig. 2. a) Series of EPR spectra of $Cu_{5.2}$MOR recorded during CH_4 oxidation at 473 K, b) double integral intensity of the EPR spectra, normalized CH_4 pressure (adapted from [23]). c) Averaged time-resolved and d) corresponding phase-resolved *operando* EPR spectra of Fe-FER during (a, b) 2-min pulses of 3 vol % O_2/Ar in a constant flow of 1000 ppm NO and 1000 ppm NH_3/Ar at 673 K (adapted from [24]). e–h), EPR-active concentration (e) and Lorentzian fraction (f) of carbonaceous deposits in the used catalysts as a function of time on stream in methanol to hydrocarbons (MTH) and methyl chloride to hydrocarbons (MCTH) as determined using CW EPR. g,h) 2D HYSCORE spectra of the zeolite after 2 h on stream for MTH (g) and MCTH (h). The insets depict the representative molecular structures of the carbonaceous species (adapted from [25]).

In a separate study, a flow-through cell was implemented and used to investigate the NO reduction by NH_3, catalyzed by Fe-exchanged ferrierite.[24] Here we applied the modulated excitation method, experimentally consisting in pulsing the O_2 gas over the zeolite equilibrated in a constant NO/NH_3 flow. This enabled phase-sensitive detection, leading to a significant improvement in signal-to-noise ratio (SNR) and time resolution (Fig. 2c-d). Thus, we could distinguish different Fe^{3+} species (d^5, S=5/2), differentiate their activity and assign them as active sites and spectator

species. Specifically, while the rhombic Fe^{3+} sites and Fe clusters were shown to be involved in reversible dynamical redox processes, upon O_2 pulses, the axial Fe^{3+} sites turned out to be virtually unreactive and after initial reduction largely stayed in the Fe^{2+} state.

In some cases, metal-free zeolites can be also investigated by EPR, as for instance for methyl coupling reactions, catalyzed by HZSM-5, specifically methyl chloride to hydrocarbons (MCTH) and methanol to hydrocarbons (MTH) for olefin production.[25] In these cases, a pool of polyaromatic radicals in a carbonaceous solid (coke) is a byproduct of the reaction. CW and pulse relaxation *ex situ* measurements of the catalyst after different times on stream shed light on coke formation and growth for the two reactants. The 2D pulse EPR technique HYSCORE, supported by DFT, provided information on changes in coke composition during the reaction. The spectra showed that aromatic radicals initially grow linearly, forming short polyacenes with up to around five condensed aromatic rings, whereas extended 2D structures are formed at long times on stream (around 60 h). Moreover, the quantitative analysis of EPR signal lineshape and amplitude (Fig. 2e-f), together with HYSCORE spectra (Fig. 2g-h), showed that coking is more prominent when methyl chloride is used, while shorter and more alkylated polyacenes are formed from methanol. These results, combined with the outcome of photoelectron photoion coincidence (PEPICO) spectroscopy, allowed for the two main mechanistic routes for the methyl coupling reaction to be proposed.

The coke signal is clearly visible at reaction temperatures and an *operando* study on coke-producing reactions is being carried out in ongoing work.

2.3 *Metal Oxide Catalysts*

A second class of catalytic system, extensively investigated by means of *operando* EPR in our group, are the metal oxides. We mainly focus on the CO_2 to methanol hydrogenation reaction. The activity and selectivity of these catalysts depend on several factors, the main ones being the ability to coordinate and activate CO_2 and to split hydrogen. The first task is commonly assumed to be carried out by oxygen vacancy defects, which function as active sites. For the second aim, metal promoters are typically used as dopants. While, as shown previously in this section, metal ions are clearly amenable to EPR investigation, oxygen vacancies can also become paramagnetic and EPR-active by trapping unpaired electrons. We investigated a broad range of catalysts, mostly based on In_2O_3 and ZnO, both pure and doped with different metal promoters (Cu, Pd, Ni), using ZrO_2 as a support.[22,26,27] With EPR measurements carried out in reaction conditions (high temperature, high pressure, continuous CO_2/H_2 flow) we were able to detect and monitor the signals from both transition metal promoters and isolated paramagnetic vacancies, as well as Zr^{3+} signals from the support. This allowed us to get a mechanistic understanding of the vacancies formation and, importantly, demonstrated the vital role of the support in the vacancies redox dynamics. Interestingly, it has been shown that the narrow EPR signals typically assigned to paramagnetic oxygen vacancies, do not correlate with the catalytic activity of the investigated systems. As also suggested by DFT, this is due to the intrinsically lower activity of the single filled, EPR-active vacancies, compared to the empty diamagnetic ones. However, very distinct broad features have been identified for the first time, which were assigned to vacancy-bound exchange-coupled magnetic polarons. These signals appear at particularly high vacancy concentrations and were shown to contribute much more to the total number of vacancies. The amplitude of these signals correlates much better with the catalytic activity. Unequivocal assignment of these signals has only been possible thanks to *operando* EPR experiments, in which the catalyst was sequentially exposed to H_2 and CO_2 (Fig. 1d-f).

3. Current Challenges and Recent Developments

Detecting signals from paramagnetic species of interest, *e.g.* transition metal centers, and distinguishing the active sites from spectator species can be challenging, especially if the concentration of active centers is low and temperatures are high (above 373 K). This is, on the one hand, related to the small Boltzmann population difference (~ 0.0016 at 298 K) of the EPR transitions, which is inversely proportional to temperature. Further challenges arise from the increased relaxation rate and the typical very broad spectrum of transition metal ions at typical reaction temperatures. Therefore, the SNR is usually low and hampers the differentiation of superimposed signals. This is especially relevant when studying complex catalytic systems with multiple active sites, which exhibit different dynamical behavior. The low SNR typically observed in *operando* EPR spectra leads to low time resolution. On a commercial EPR spectrometer, the time of a field scan is limited by the sweep and stabilization time of the electromagnet as well as the signal-to-noise ratio. High-time resolution however is crucial for capturing rapid spectral changes during a reaction. Therefore, it can be challenging to balance time resolution with signal intensity, and *operando* EPR setups face limitations in capturing fast kinetic processes. These challenges can be addressed by the development of new instrumentation and detection schemes. In the next paragraph, we will give an overview of our efforts.

Recently, we introduced modulated excitation spectroscopy as a new detection scheme in *operando* EPR, which allows us to tackle the issues of low SNR while detecting broad spectra. Due to the consecutive time averaging of multiple reaction cycles, the SNR can be improved without sacrificing time resolution, which turns out to be beneficial.[24]

3.1 *Design Principles of High-temperature Resonators*

Besides development of new detection schemes, hardware development is important in order to improve SNR and time resolution. In EPR, unlike most other spectroscopic methods, the design of the spectroscopic cell, or ideally a reactor, is constrained by the need to employ a microwave resonator. Therefore, resonator design must go hand in hand with methodology development. Due to the lack of suitable commercial equipment, our group has developed over the last years different high-temperature X-band resonators. The resonant frequency is governed by the physical dimensions of the resonator, which imposes limitations on the design of the spectroscopic cell. Therefore, besides one notable exception[1] high-temperature resonators are usually restricted to the X-band (9-10 GHz), where the wavelength of ~3 cm is more compatible with the needs of the reaction cell than at higher frequencies. The design of new resonators not only needs to account for the properties that are required for the microwave cavity but also has to be compatible with high-temperature measurements and product detection. Therefore, the design was guided by the following principles.

- Dimension and shape: The size and the shape of the resonant structure of the cavity needs to be designed such that with the large double walled quartz dewar needed for the heating the frequency is in the accessible range of standard X-band bridges which is typically around 9.1-9.9 GHz.
- Quality factor and filling factor: The EPR signal is directly proportional to the filling factor η and the quality factor Q.[28] Resonance means that the cavity stores a small amount of microwave energy; therefore, if the resonator is 'perfectly' coupled (called critical coupling), no microwaves are reflected. Resonators are characterized by their quality factor Q, which indicates how efficiently the cavity stores microwave energy rather than dissipating it. The resonator Q is therefore defined as the ratio between the energy stored in the resonator and the energy lost per cycle. The filling factor η can be approximated by the ratio of the sample volume to the cavity volume, whereas the exact value is obtained by integration over vol-

ume that considers the spatial distribution of the amplitude of the magnetic component of the microwave field. Inherently, a higher filling factor makes the resonance frequency of the cavity more sensitive to the position of the sample tube, because the electric component of the microwave field is separated from the magnetic component only on the order of sample dimension. Since simultaneous optimization of both filling factor and *Q* factor is not feasible, in the design one of these is optimized (see discussion below).

- Cooling: Cooling of the resonator walls and the modulation coils is one of the most crucial aspects of designing high-temperature resonators. Insufficient cooling results in a drifting resonance frequency of the cavity and in reduction of its *Q* factor, which makes measurements tedious and less sensitive. Therefore, in our design water cooling plates cool the resonator walls and the modulation coils. Temperature variation at the modulation complicates control of microphonics. Such vibration of the modulation coils manifests as large spikes in the spectrum, which prevents the acquisition with an acceptable signal-to-noise ratio.
- High and stable temperature: Equally important to stable cooling of the resonator walls and modulation coils is stable heating and temperature at the sample. In principle, two different types of heating are possible: (1) Heating with a stream of hot gas, typically N_2,[14,19] or (2) heating with metal wires *e.g.* Pt mounted at the outside of the quartz dewar at the position of the catalyst bed.[11,29] The latter one becomes impractical if different samples need to be measured in a short amount of time since every sample change requires dismounting the resonator and cleaning the heatable tube. With gas-stream heating it is more challenging to reach high temperatures. For that, the connection between the gas heater gas and the sample tube must be as short and straight as possible, and the flow of the heating gas must be optimized. Therefore, we mount the heater directly under the cavity. That way we can achieve temperatures up to 900 K. On the other hand, this design complicates gas flow geometry.
- Minimal temperature gradient: In addition to achieve a stable temperature, we need to attain a small temperature gradient over the catalyst bed. A large gradient leads to less well defined kinetics and to different reactivity at different points in the bed. Direct heating with platinum wires has the advantage that the heater uniformly affects the entire catalyst bed. However, if the gas flowing through the bed is not heated beforehand, it will introduce a gradient because it must be heated up by the catalyst. Heating with hot air or N_2 causes a temperature difference of about 10-20 K between the entry and outlet of the catalyst bed. The amount of catalyst is limited as this temperature difference increases with increasing sample height. We have tried to minimize temperature differences by employing a double walled quartz dewar to isolate the hot gas from cooling as much as possible.

3.2 *High-temperature Resonators*

We have designed and built two different high-temperature cavities (Fig. 3). The cooling plates and heat dispersive elements as well as the heater and the thermocouple are highlighted. The resonator depicted in Fig. 3a is based on a rectangular TE102 cavity design, while the one pictured in Fig. 3b is based on a cylindrical TE011 cavity. The latter one has already been successfully employed in *operando* EPR measurements (Fig 3b).[19,21]

Due to the geometrical differences, the resonators exhibit different *Q* and filling factor values. While the rectangular cavity possesses a relatively low *Q* value of about 3000, the cylindrical shaped resonator exhibits a high *Q* value of about 10000. The filling factor of the rectangular cavity is 0.8%, and 2.0% for a sample height of 0.5 cm and 2 cm respectively. Likewise, for the same sample dimension the filling factor for the cylindrical cavity is 1.1% and 3.6%. For both resonators we evaluated the distribution of the magnetic component of the microwave field through measurements of a small standard 2,2-diphenyl-1-picrylhydrazyl (DPPH) sample. The results are depicted in Fig. 4a. The rectangular cavity shows a much smaller active volume than the cylindrical one. Further, the performance of both resonators was tested (see Fig. 4b). As is evident by the measurements of a $Cu(pic)_2$:$Zn(pic)_2$ standard sample, the rectangular cavity has about a 5 times weaker signal to noise ratio, which can be explained by the lower *Q* value and a smaller filling factor. The sample employed has a filling height of about 0.5 cm, which is a typical sample volume for *in situ*/*operando* measurements. The corresponding simulations of the B_1 and E_1 field of both resonators can be found in Fig. 5. The B_1 and E_1 distribution in the rectangular resonator suggests that it exhibits lower dielectric losses, compared to the cylindrical one, if the sample is conductive or otherwise lossy. This means that the choice of the resonator may be strongly affected by the dielectric properties of the sample. In particular, for conducting or otherwise lossy samples, the rectangular resonator would allow the use of flat sample cells, whereas sample volume would need to be reduced drastically with the cylindrical resonator.

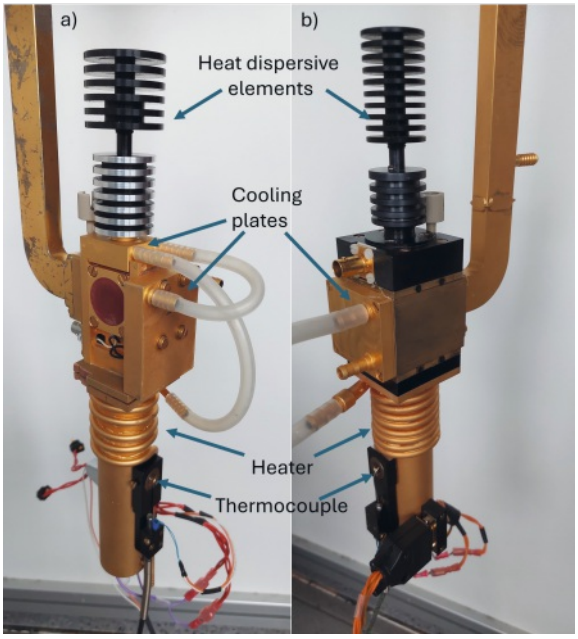

Fig. 3 a) Rectangular high-temperature resonator b) cylindrical high temperature resonator.

Another difference between the resonators is the improved cooling circuit of the rectangular resonator. As evident in Fig. 3a, this resonator features a large front cooling plate in comparison to the cavity volume as well as a cooling plate on top of the resonator. Further, the outside of the heater tube is cooled. This improvement leads to extremely stable frequency, which allows for ramping the temperature from room temperature up to 800 K without the need to retune the resonator and therefore for automated temperature ramps. Further, the cooling allows for modulation amplitudes of over 5 G at 700 K. The cylindrical resonator has cooling only at the front of the cavity and at the outside of the heater. This results in the necessity to retune the instrument manually during temperature ramps and further restricts the modulation amplitude to 1-2 G at 700 K.

Besides these differences, the heating system of both resonators is the same. The heated N_2 gas is flowing from the bottom. Therefore, the gases have to flow through a U-shaped tube (see Fig. 1). Two different geometries are possible. In the first geometry, the gas flows through the inner tube into the catalyst bed. The products subsequently leave through the outer capillary

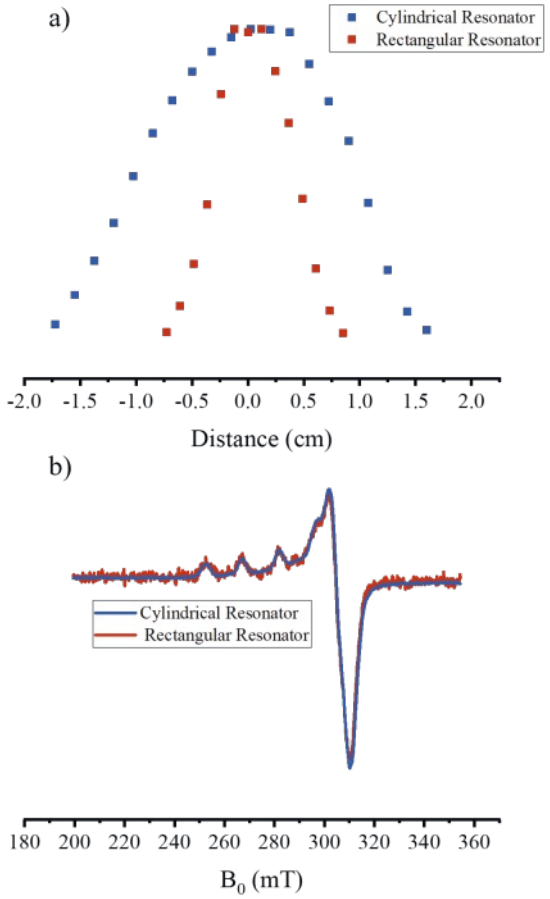

Fig. 4a) Dependence of signal amplitude of a DPPH sample on vertical distance from the cavity center for the two high-temperature resonators, measured at room temperature b) Comparison of the two resonators. The measurement was performed at room temperature on a $Cu(pic)_2$:$Zn(pic)_2$ sample containing 0.4 w-% Cu^{2+}.

toward a mass spectrometer. In the second geometry the catalyst bed is fixed in the inner capillary, and the gas enters the bed from below. The latter configuration presents several advantages. First, the gases are preheated by contacting the hot quartz wall during the flow down. Furthermore, the interaction between the catalysts and the gas is maximized, as the latter passes through the former. Finally, using thinner capillaries allows samples with higher conductivity to be measured. The main drawback of this geometry is the lower amount of sample which can be employed for the measurements. Therefore, the optimal choice of setup depends on the sample.

4. Conclusion and Future Directions

In this article, we summarized recent developments in our group in *operando* EPR and discussed some technical aspects. The examples given demonstrate the broad applicability of *operando* EPR not only towards reactive isolated species but also for magnetically coupled systems. Moreover, the studies carried out demonstrate the importance to perform spectroscopy under reaction conditions to differentiate between active and inactive species.

An inherent problem of X-band EPR is the differentiation between species that exhibit spectral overlap, especially at low signal-to-noise ratio. For this, routine measurements at higher frequencies would be beneficial to improve spectral resolution. The practicality of such measurements was so far hampered by the small dimension of the cavity and correspondingly small sample volume. In recent years commercial Q-band resonators for CW EPR were developed that accommodate oversized samples with 3 mm outer diameter, such as the ER5106QT-2 from Bruker Biospin. These resonators overcome the limitation at least partially and put the development of similar high-temperature Q-band cavities within reach.

One key advantage of EPR is its sensitivity towards the chemical surrounding of the catalytic site and the possibility to detect magnetic nuclei in close proximity. Unfortunately, this information is often lost in CW EPR due to line broadening. Pulsed EPR experiments can separate and thus resolve smaller interactions but are usually not feasible at high temperature due to fast electron spin relaxation. Coal and coke are noticeable exceptions, where

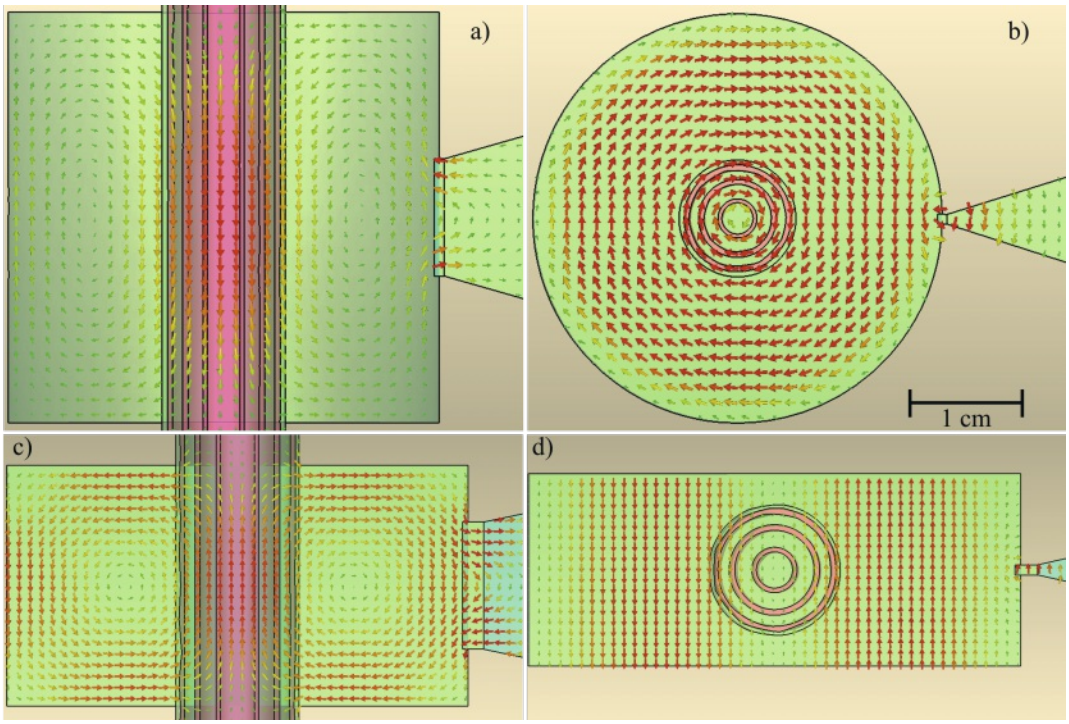

Fig. 5 a) Strength of the *z*-component of the B_1-field in a vertical cross-section through the cylindrical cavity centre b) Strength of the *z*-component of the E_1-field in a horizontal cross-section of the cylindrical cavity at the level of the iris. c) and d) show the same fields for the rectangular cavity. The colour gradient ranges from green (low field) to red (high field).

electron spin echos are typically observable at least at room temperature. Alternatively, small hyperfine interactions can be resolved by CW electron nuclear double resonance (ENDOR). In ENDOR, CW radiofrequency irradiation is used in combination of CW microwave irradiation to elucidate the type of nuclei which are in close proximity to the electron. Due to simultaneous irradiation and detection, CW ENDOR is feasible at faster relaxation of the electron spin, as long as the ratio of electron and nuclear relaxation rates is favorable. However, even this technique may be limited to moderate temperatures and organic radicals, such as the ones featuring in coke or in pyrolysis processes.

Finally, new combinations of *operando* EPR with other techniques can be explored, such as conductivity and advanced optical measurements, which would provide a more complete understanding of the catalytic mechanisms.

Acknowledgements

The authors want to express their gratitude towards their multiple collaboration partners within ETH Zurich and PSI. We specially thank Javier Pérez-Ramírez, Jeroen van Bokhoven, Sharon Mitchell, Cecilia Mondelli, Davide Ferri, Vitaly Sushkevich, and Daniel Klose. MA acknowledges funding for this work by NCCR Catalysis. JF acknowledges funding for this work by the ETH Research Grant ETH-48 20-1.

Received: March 13, 2024

[1] A. Brückner, *Chem. Soc. Rev.* **2010**, *39*, 4673, https://doi.org/10.1039/B919541F.
[2] A. Brückner, *Catal. Rev.* **2003**, *45*, 97, https://doi.org/10.1081/CR-120015739.
[3] A. Brückner, *Phys. Chem. Chem. Phys.* **2003**, *5*, 4461, https://doi.org/10.1039/B305884K.
[4] S. A. Bonke, T. Risse, A. Schnegg, A. Brückner, *Nat. Rev. Methods Primers* **2021**, *1*, 1, https://doi.org/10.1038/s43586-021-00031-4.
[5] S. K. Misra, S. Diehl, D. Tipikin, J. H. Freed, *J. Magn. Reson.* **2010**, *205*, 14, https://doi.org/10.1016/j.jmr.2010.03.013.
[6] J. Krzystek, A. Ozarowski, J. Telser, *Coord. Chem. Rev.* **2006**, *250*, 2308, https://doi.org/10.1016/j.ccr.2006.03.016.
[7] V. A. Bolshov, A. M. Volodin, *React. Kinet. Catal. Lett.* **1991**, *43*, 87, https://doi.org/10.1007/BF02075417.
[8] P. L. Corio, S. Shih, *J. Catal.* **1970**, *18*, 126, https://doi.org/10.1016/0021-9517(70)90170-3.
[9] H. G. Karge, J.-P. Lange, A. Gutsze, M. Łaniecki, *J. Catal.* **1988**, *114*, 144, https://doi.org/10.1016/0021-9517(88)90016-4.
[10] Y. Kurita, T. Sonoda, M. Sato, *J. Catal.* **1970**, *19*, 82, https://doi.org/10.1016/0021-9517(70)90299-X.
[11] J.-P. Lange, A. Gutsze, H. G. Karge, *J. Catal.* **1988**, *114*, 136, https://doi.org/10.1016/0021-9517(88)90015-2.
[12] J. Rabeah, V. Briois, S. Adomeit, C. La Fontaine, U. Bentrup, A. Brückner, *Chem. Eur. J.* **2020**, *26*, 7395, https://doi.org/10.1002/chem.202000436.
[13] J. Rabeah, J. Radnik, V. Briois, D. Maschmeyer, G. Stochniol, S. Peitz, H. Reeker, C. La Fontaine, A. Brückner, *ACS Catal.* **2016**, *6*, 8224, https://doi.org/10.1021/acscatal.6b02331.
[14] A. Brückner, E. Kondratenko, *Catal. Today* **2006**, *113*, 16, https://doi.org/10.1016/j.cattod.2005.11.006.
[15] A. Godiksen, F. N. Stappen, P. N. R. Vennestrøm, F. Giordanino, S. B. Rasmussen, L. F. Lundegaard, S. Mossin, *J. Phys. Chem. C* **2014**, *118*, 23126, https://doi.org/10.1021/jp5065616.
[16] A. L. Godiksen, M. H. Funk, S. B. Rasmussen, S. Mossin, *ChemCatChem* **2020**, *12*, 4893, https://doi.org/10.1002/cctc.202000802.
[17] M. Seif-Eddine, S. J. Cobb, Y. Dang, K. Abdiaziz, M. A. Bajada, E. Reisner, M. M. Roessler, *Nat. Chem.* **2024**, *1*, https://doi.org/10.1038/s41557-024-01450-y.
[18] Y. Kutin, N. Cox, W. Lubitz, A. Schnegg, O. Rüdiger, *Catal.* **2019**, *9*, 926, https://doi.org/10.3390/catal9110926.
[19] C. Bährle, V. Custodis, G. Jeschke, J. A. van Bokhoven, F. Vogel, *ChemSusChem* **2014**, *7*, 2022, https://doi.org/10.1002/cssc.201400079.
[20] C. Bährle, V. Custodis, G. Jeschke, J. A. van Bokhoven, F. Vogel, *ChemSusChem* **2016**, *9*, 2397, https://doi.org/10.1002/cssc.201600582.
[21] G. Zichittella, Y. Polyhach, R. Tschaggelar, G. Jeschke, J. Pérez-Ramírez, *Angew. Chem. Int. Ed.* **2021**, *60*, 3596, https://doi.org/10.1002/anie.202013331.
[22] T. Pinheiro Araújo, C. Mondelli, M. Agrachev, T. Zou, P. O. Willi, K. M. Engel, R. N. Grass, W. J. Stark, O. V. Safonova, G. Jeschke, S. Mitchell, J. Pérez-Ramírez, *Nat. Commun.* **2022**, *13*, 5610, https://doi.org/10.1038/s41467-022-33391-w.
[23] J. W. A. Fischer, A. Brenig, D. Klose, J. A. van Bokhoven, V. L. Sushkevich, G. Jeschke, *Angew. Chem. Int. Ed.* **2023**, *62*, e202303574, https://doi.org/10.1002/anie.202303574.
[24] J. W. A. Fischer, F. Buttignol, A. Brenig, D. Klose, D. Ferri, V. Sushkevich, J. A. van Bokhoven, G. Jeschke, *Catal. Today* **2024**, *429*, 114503, https://doi.org/10.1016/j.cattod.2023.114503.
[25] A. Cesarini, S. Mitchell, G. Zichittella, M. Agrachev, S. P. Schmid, G. Jeschke, Z. Pan, A. Bodi, P. Hemberger, J. Pérez-Ramírez, *Nat. Catal.* **2022**, *5*, 605, https://doi.org/10.1038/s41929-022-00808-0.
[26] T. Pinheiro Araújo, J. Morales-Vidal, T. Zou, M. Agrachev, S. Verstraeten, P. O. Willi, R. N. Grass, G. Jeschke, S. Mitchell, N. López, J. Pérez-Ramírez, *Adv. Energy Mater.* **2023**, *13*, 2204122, https://doi.org/10.1002/aenm.202204122.
[27] T. Zou, T. Pinheiro Araújo, M. Agrachev, X. Jin, F. Krumeich, G. Jeschke, S. Mitchell, J. Pérez-Ramírez, *J. Catal.* **2024**, *430*, 115344, https://doi.org/10.1016/j.jcat.2024.115344.
[28] G. R. Eaton, S. S. Eaton, D. P. Barr, R. T. Weber, 'Quantitative EPR', Springer, Vienna, **2010**, https://doi.org/10.1007/978-3-211-92948-3.
[29] A. Brückner, B. Kubias, B. Lücke, *Catal. Today* **1996**, *32*, 215, https://doi.org/10.1016/S0920-5861(96)00077-6.

License and Terms